Hindawi
Advances in Materials Science and Engineering
Volume 2023, Article ID 5523162, 14 pages
https://doi.org/10.1155/2023/5523162

Research Article

A Comparative Analysis among Quenched, Tempered, and Stepped Cooled TIG Welded SS-304 Plates Based on Tensile Strength, Hardness, and Microstructural Appearance

Saurabh Dewangan,[1] **Saksham Saksham**,[1] **Adhir Chandra Paul**,[2] **and Jaka Burja**[3]

[1]*Department of Mechanical Engineering, Manipal University Jaipur, Jaipur 303007, Rajasthan, India*
[2]*Department of Leather Engineering, Faculty of Mechanical Engineering, Khulna University of Engineering and Technology, Fulbarigate, Khulna 9203, Bangladesh*
[3]*Institute of Metals and Technology, 1000 Ljubljana, Slovenia*

Correspondence should be addressed to Adhir Chandra Paul; acpaul@le.kuet.ac.bd

Received 28 January 2023; Revised 22 March 2023; Accepted 3 April 2023; Published 14 April 2023

Academic Editor: Fuat Kara

The present experimental work critically analyses the changes in microstructural orientation and mechanical properties of TIG (tungsten inert gas) welded AISI-304 (SS) plates which have undergone through various heat treatments. The characteristics of heat-treated samples have been compared with those of untreated samples which is denoted by the original sample in this study. Five SS-304 plates were welded by the TIG method. Out of five, four plates were heat treated and one plate was put in the original condition. Four heat treatment includes quenching, stepped heat treating (sand + water), tempering-1 (quick quench then sand cooling), and tempering-2 (quick quench then air cooling). In all the five plates, the tensile test and microhardness test have been performed. In addition, microscopic observation of cross-sectional surfaces has also been carried out. The base metal (BM) zone of all five plates mainly consists of equiaxed γ-grains, although twin can be observed only in the original sample. The heat-affected zone (HAZ) imparts both lathy and dendritic type δ-ferrite at the transition of the BM and welded zone (WZ). At the welded zone, the γ-matrix has become coarse with numerous spots and dendrites of δ-ferrite could be seen. Sample 3, tempered by means by water sprinkling for a very short time and then cooling in sand, has shown satisfactory results among all. The sample has achieved the 23% higher extension value and 10% higher hardness at WZ than these of the original sample, although a negligible loss (0.2%) of ultimate tensile strength (UTS) is also reported in sample 3.

1. Introduction

Metallography of AISI-304 steel, i.e., austenitic stainless steel (grade 304) has been taken under study by many researchers because of wide range of applications of this metal. This steel is alloyed with 8% Cr and 10% Ni which makes it highly corrosion resistant [1]. This grade of steel possesses lowers conductivity to heat and electricity than low-carbon steel. It is easy to mould it into different forms. SS-304 is widely utilized in the automobile, ship building, chemical plants, aircrafts, and construction areas [2]. SS-304 imparts a good weldability, and it can be conveniently welded by fusion welding techniques such as gas metal arc welding and gas tungsten arc welding. SS-304 has been widely explored with respect to its performance under different welding conditions which include similar and dissimilar metal joints [3], varying yield parameters [4], and postweld heat treatments [5]. Welding is an old but very important part of fabrication processes. In the present scenario, research on welding and its analysis is still happening. Mostly metals such as Al, Ti-alloys, and different grades of steels have been thoroughly analyzed by the researchers to enhance their application range in industries [6, 7]. The importance of heat treatment to metals has also been extensively discussed to modify the mechanical properties such as strength [8], hardness [9], bending strength [10], toughness [11], and ductility [12].

Some of the previous works on welding and heat treating of steel are discussed as follows.

In a work, 55Si7 grade, a medium carbon steel, was taken into consideration for welding followed by heat treatments. As a result, a considerable decrement in hardness was achieved and the heat affected zone was found as the lowest hard area in the plate [13]. Another grade, i.e., 120-Mn_3Si_2 steel was considered for analyzing the properties of the welded joint after heat treatment. Welded plates were quenched in water, and because of that, austenite was formed as layers in the welded joint. In addition, the residual austenite was reported in between the layers which further lead to formation of martensite. The result was obtained as a low value of tensile strength (i.e., 209.27 MPa) of the welded joint [14]. The effects of thermal aging at 400°C up to 10000 hours were investigated in welded joints of two metals, i.e., low alloy steel (SA 508) and nickel-based alloy steel (Alloy 52). SA508 is a ferritic type of steel, whereas Alloy 52 is an austenitic steel. Postweld treatment had not significantly affected the properties of the base metal and heat affected zone. The transition of two metals had been influenced by aging. It was seen that carbon had diffused from the welded zone to away from the weld centre line. Therefore, a reduction in hardness was reported in the welded zone [15]. The metal inert gas (MIG) welding technique was used to deposit the SS-304 layer on Q235 carbon steel for enhancing the physical properties of low-carbon steel, i.e., Q235. Both the welded joint and deposited surface were free from any type of defects. The surface was mainly composed of martensite along with traces of ferrite and austenite. It was observed that the deposited layer surface and the welded joint were highly corrosion resistant as compared to carbon steel alone, although the hardness of the layer was found lower than the welded joint [16]. Dissimilar steels such as stainless and structural grades were welded and analyzed through microscopes and various mechanical tests to examine the reliability of joints. It was seen that 308LSI steel was found suitable as a filler rod for the welding process. The tensile test was performed to check the strength of the joint. It was noticed that the joints possess an average strength of 472 MPa. The area of the heat-affected zone was too high to cause fracture over there during the tensile test [17]. In an experimental work, it was noted that a significant reduction in weld penetration and a considerable improvement in the microstructure could have happened by rotating the filler wire during its downward feeding which causes an altered fluid flow in the fusion zone. Also, the strength of the joint was greatly improved after formation of the fine microstructure in the welded zone [18]. 2205 duplex stainless was welded by the TIG method, and the welded plate was critically analyzed at five different zones from the welded zone to the base metal zone to examine the grain structure, hardness, and corrosion behavior. It was observed that the second pass of welding had created a reheating phenomenon which had caused the formation of secondary austenite in the welded zone. Also, the coarse ferrite had come closer to the fusion line. Austenite was found tougher than ferrite from the weld metal to the fusion zone [19]. In a work, the AISI-304 metal plate was welded by MIG welding with Ar as inert gas and 308L as the electrode material. It was observed that δ-ferrite grains started to form as soon as heat input increased beyond 1.25 kJ/mm. As a result, the ultimate tensile strength and toughness of the material got decreased in the weld region. In addition, hardness was reported at its minimum value at the welded zone. The heat-affected zone was reported as highly hard due to formation of fine grains after rapid cooling [20]. SS-304 samples had undergone through pressure quenching at 1600°C temperature and 4 GPa pressure. Microstructures of these samples contained γ-Fe (FCC) and α-Fe (BCC), which were observed by X-ray profiles. Diffraction peaks of the pressure quenched sample were wider than other samples, possible causes could be grain refinement and microstrain during the solidification process. Pressure quenched samples were found to possess better hardness and yield strength, although there was no improvement in ultimate tensile strength, and also, the rate of elongation got decreased due to the presence of large density dislocations [21].

After going through the previous literature, it has come to the notice that various grades of steels had been analyzed at different experimental conditions. Sometimes, different results could also be observed for same working conditions. SS-304, being a commercial grade of stainless steel, is widely used all over the world, and therefore, a continuous assessment is required to increase its applicability.

In this direction, the present work provides a comparative analysis among four different heat treatment processes applied over the TIG-welded plates of AISI-304 (SS-304). The tensile strength, microhardness, and grain structure are the basis of this comparative analysis.

2. Experimental Work

Step 1: Collection of SS plates and welding ⟶ experimental work involves the collection of 10 nos. of AISI-304 (SS-304) plates with dimension $50 \times 50 \times 3$ mm each. Five pairs of plates were welded in butt configuration by the tungsten inert gas (TIG) welding technique which had a tungsten electrode of 4 mm. The TIG 400 (Mosfet DC inverter) machine was utilized for welding purpose. The input parameters, i.e., voltage and current values of 25 V and 180 A, respectively, were selected for welding the plates. It was a random selection based on the suitable requirement for the 3 mm thick SS plate. The filler rod of SS-304 was selected in the form of a 2 mm thick wire. The "V" groove of 45° was created on the edges of two adjoining surfaces. Welding was carried out on both sides of the plate. During welding, arc shielding was carried out by providing argon gas (purity > 99%) with an identification number Ar 5.0. The flow of argon gas was maintained at 11.5 l/min. After welding, five pairs were named as sample 1, sample 2, sample 3, sample 4, and sample 5.

Step 2: Heat treatment ⟶ postweld heat treatment methods were adopted after welding the plates. Sample 1 was left as welded and named as the original sample. Rest of the samples were heated up to 900°C for 1 h in

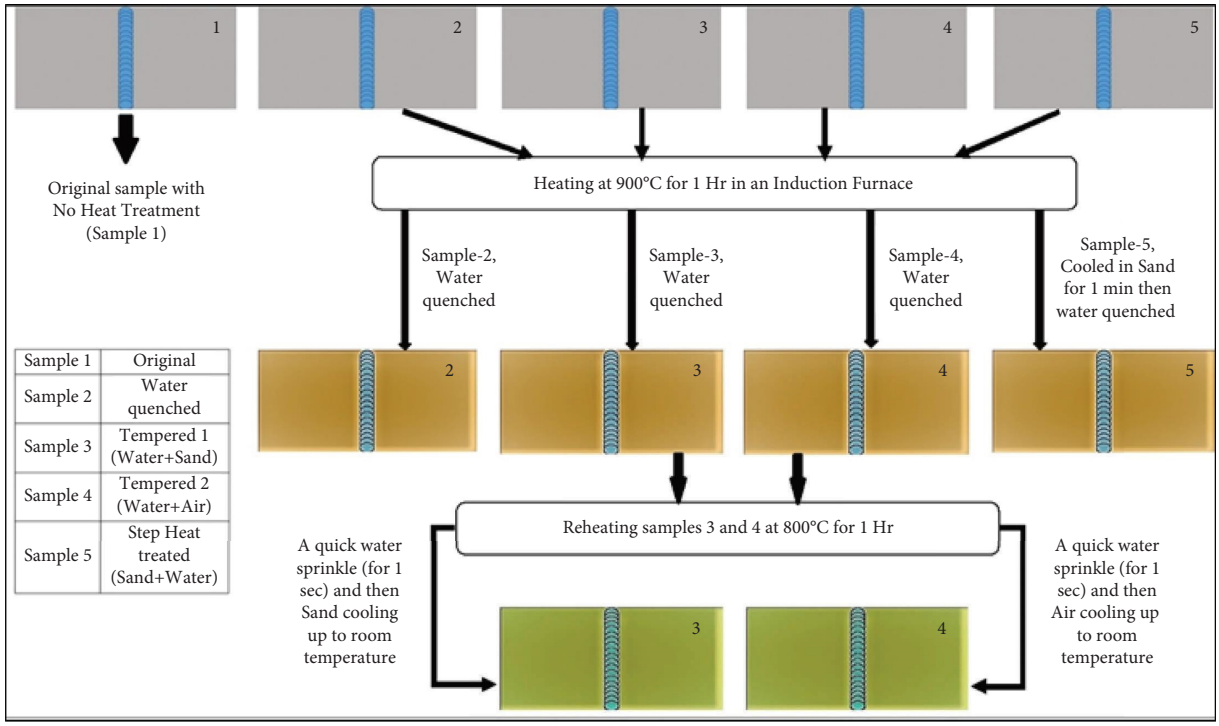

Figure 1: Outline of the experimental work including welding, heat treating, and tempering.

an induction furnace. In other words, four samples had soaked heat for 1 hour. The purpose of heating is to make the microstructure equiaxed and stress-free. Three samples, i.e., sample 2, sample 3, and sample 4 were quenched by dipping them into water. Heat treating of sample 2 became over as soon as it was quenched. It was named as water quenched. Sample 5 was cooled in two steps: first 1 min in sand (fully buried inside it) and then in water till room temperature. Hence, sample 5 is termed as the sand + water-cooled sample.

Step 3: Tempering of sample 3 and sample 4 ⟶ after quenching, both, sample 3 and sample 4 were again heated in the furnace for a holding time of 1 h. Now, the cooling methods were varied for both the samples. Sample 3 was cooled in two steps: (i) a quick water sprinkle for 1 s for possible rapid cooling of surface and (ii) then, cooling inside sand up to room temperature. Hence, sample 3 was named as the water + sand-cooled sample. Sample 4 was also cooled in two steps: (i) a quick water sprinkle for 1 s and (ii) cooling in atmospheric air. Therefore, sample 4 was indicated by the water + air-cooled sample.

To properly understand the processes of experiments, an outline is provided in Figure 1. The actual welded plates taken under the study are shown in Figure 2(a). The heat-treated samples are shown in Figure 2(b).

Step 4: Preparation of tensile test specimens ⟶ from all the five welded plates, the specimens for the tensile test were prepared by using wire-electric discharge machining. These samples were prepared as per the ASTM-E8 standard. The specimens are shown in Figure 2(c) (i).

Step 5: Preparation of samples for hardness and the microstructural test ⟶ all the plates were cut across the welded joint to make other plates of $100 \times 10 \times 3$ mm dimension. These cut sections were used for the hardness test (on one cross section) and microstructural observation (on another cross-section). The specimens are shown in Figure 2(c) (ii). The cross-sectional surfaces were properly finished for the microhardness test. For microscopic analysis, the other side of the cross-sectional surface was highly polished by using the rotating disc polisher. Five different grit sizes, i.e., 1000, 1400, 1800, 2200, and 2500 of sand papers were used for superfinishing the work. Adler's etchant (ferric chloride + copper ammonium chloride + hydrochloric acid + distilled water) was applied 1 min before the microscopic observation. All the polished samples are shown in Figure 3. Three zones, i.e., the base metal zone (which is affected by heat), welded zone (gets converted in molten state), and heat-affected zone (not melted by highly heated) were focused for any microstructural changes.

Step 6: Tensile testing ⟶ the tensile test was conducted on a universal testing machine which was controlled by the hydraulic system. There was a data acquisition system attached to it so that the load-displacement curve could be recorded during the test. The strain rate of 0.001 s^{-1} was selected for the test. All the specimens got fractured through the welded

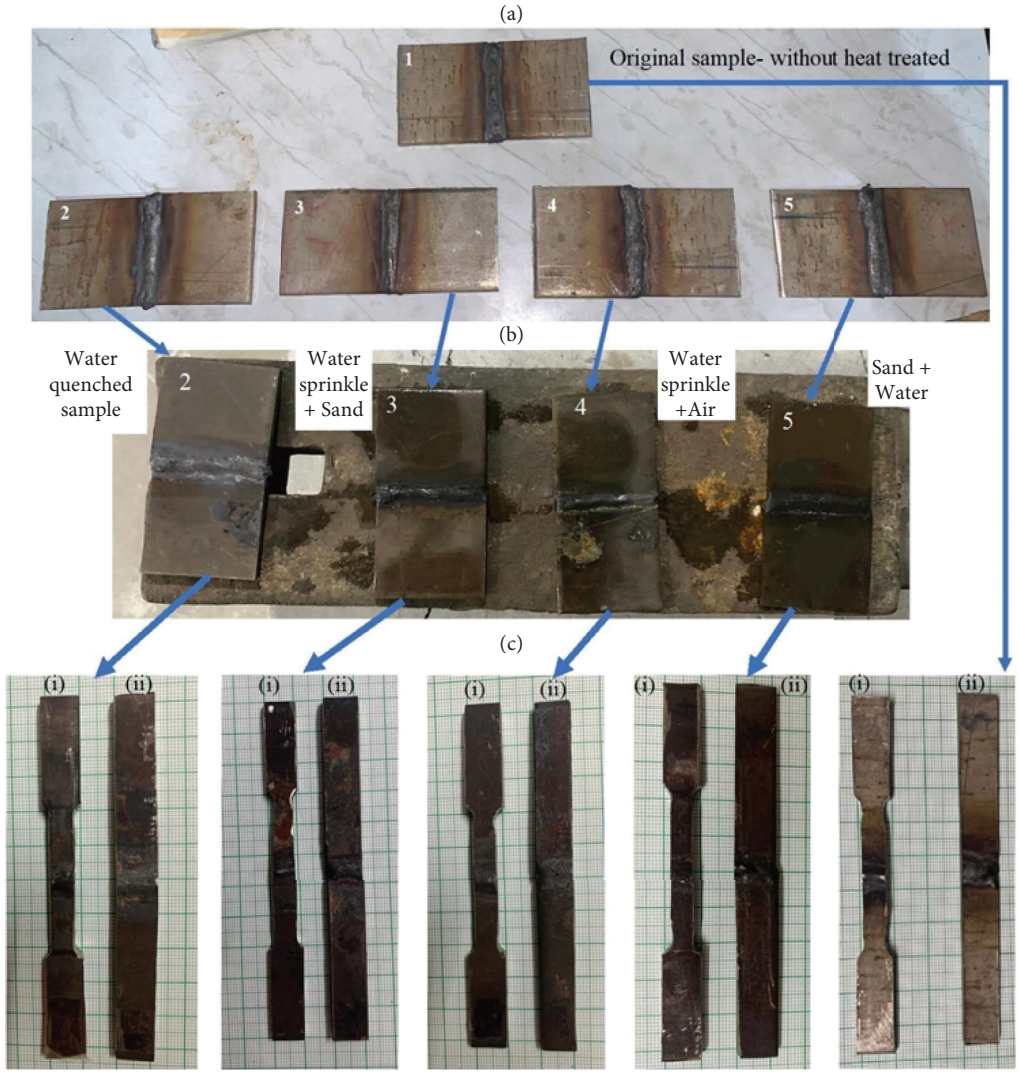

(i) Tensile test specimens prepared from five welded plates;

(ii) Samples for micro-hardness test on one cross sectional surface and Microstructural observation on other cross sectional surface.

Figure 2: Details of experimental work: (a) five welded plates indicated by 1, 2, 3, 4, and 5; (b) four heat-treated plates; (c) (i) the tensile test specimens; (ii) specimens for hardness and the microscopic test.

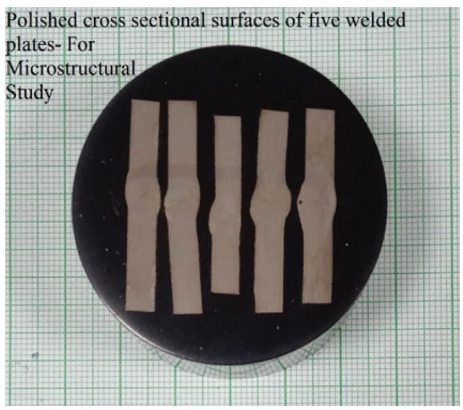

Figure 3: Five polished samples for microscopic analysis.

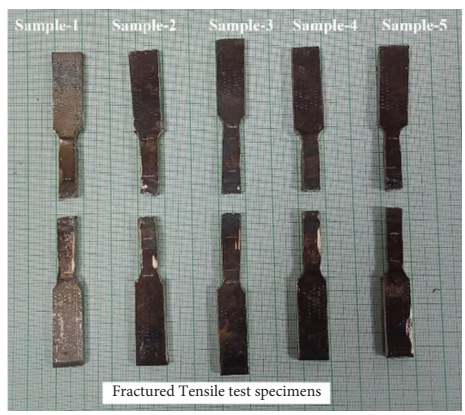

Figure 4: Broken tensile test specimens.

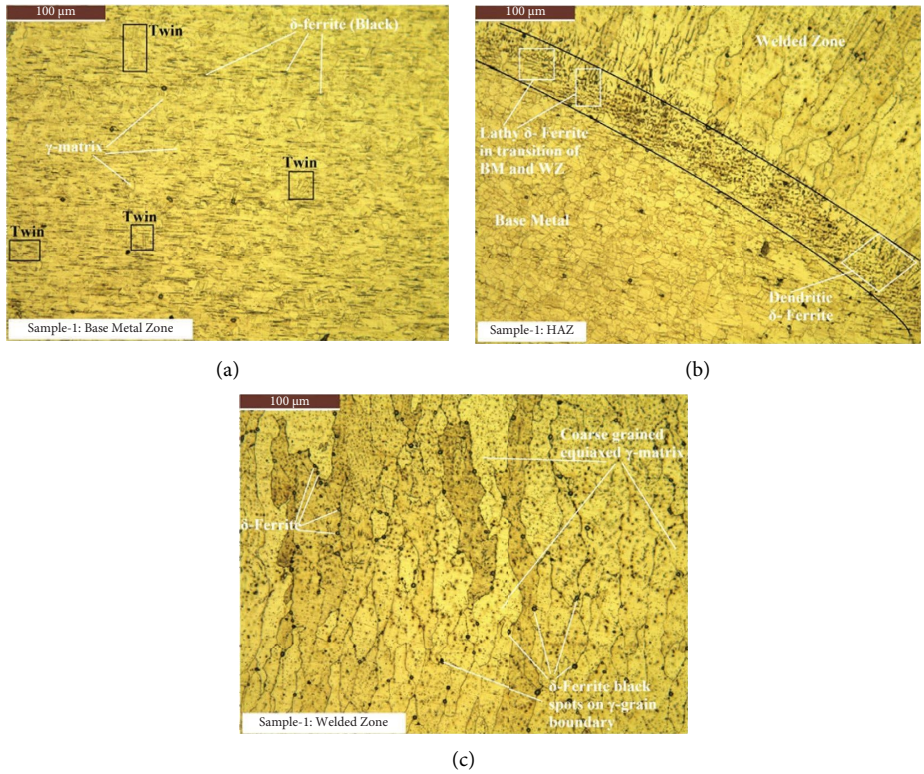

Figure 5: Microstructural appearance of sample 1 (original sample): (a) the base metal, (b) HAZ, and (c) welded zone.

joint during the tensile test. The broken tensile test specimens are given in Figure 4.

Step 7: Fractographic testing of broken specimens ⟶ the fractured parts of the used tensile test specimens were cut by the EDM method in such a way that the height of each sample should not exceed 5 mm. These samples were, then, observed through the field emission scanning electron microscope (FESEM). The central part of the fractured area was focused for capturing the images.

Step 8: Hardness testing ⟶ the Vickers microhardness test was conducted on each welded plate to know the variation of hardness among three zones, i.e., the base metal zone, welded zone, and heat-affected zone. A load of 300 gm was considered for the test.

3. Result Analysis and Discussion

The outcomes of the tests conducted are discussed in this section.

3.1. Microstructural Test Results. The SS-304 grade is known as austenitic steel in which main alloying elements are Cr and Ni apart from Fe. It contains mainly austenite (FCC) and ferrite (BCC) based on the circumstances of solidification. If solidification happens in the equilibrium condition; then, the final microstructure will be mostly γ-austenite. If solidification is nonequilibrium, there is variation in the cooling rate or in case of rapid cooling, and then, the transformation from δ-ferrite to γ-austenite does not take place fully. In this case, a metastable δ-ferrite may remain with the γ-matrix [22]. In general, the austenitic steel like SS-304 may contain 2–10% of δ-ferrite, especially in the case of the weld metal. Due to the presence of the δ-phase, the occurrence of embrittlement and hot cracking is avoided during solidification of weldment [23].

All the microstructural images in this study were captured at a scale of 100 μm and a magnification of 100X. The microstructures of sample 1 are shown in Figures 5(a)–5(c). Figure 5(a) depicts the grains in the base metal part in which a fine the γ-matrix could be seen surrounded by δ-ferrite in the boundaries of the γ phase. Some of the δ-phases are linear and a very small number of δ-ferrite globules could be noted. It is the only sample where twins could be properly seen in the base metal zone. The γ-matrix, δ-ferrite, and twins are indicated in Figure 5(a). Figure 5(b) shows the HAZ in which the boundary between BM and WZ is clearly indicated by black colored lines. It is the area where the microstructure is completely different from BM and WZ. Despite having the coarse, fine, and equiaxed structure, this zone contains the lathy $(\delta + \gamma)$ structure at one part and some dendritic structures at another part. Figure 5(c) shows WZ, where γ-austenite is significantly coarser than that of BM. The distribution of δ-ferrite is mainly in the form of globules and spots. Some lathy-type δ-ferrite appearance can also be noticed in the image.

The microstructure of sample 2 is explained in Figure 6. Figure 6(a) is an image of BM which is completely different from the same of sample 1. In this, the γ-matrix is equiaxed

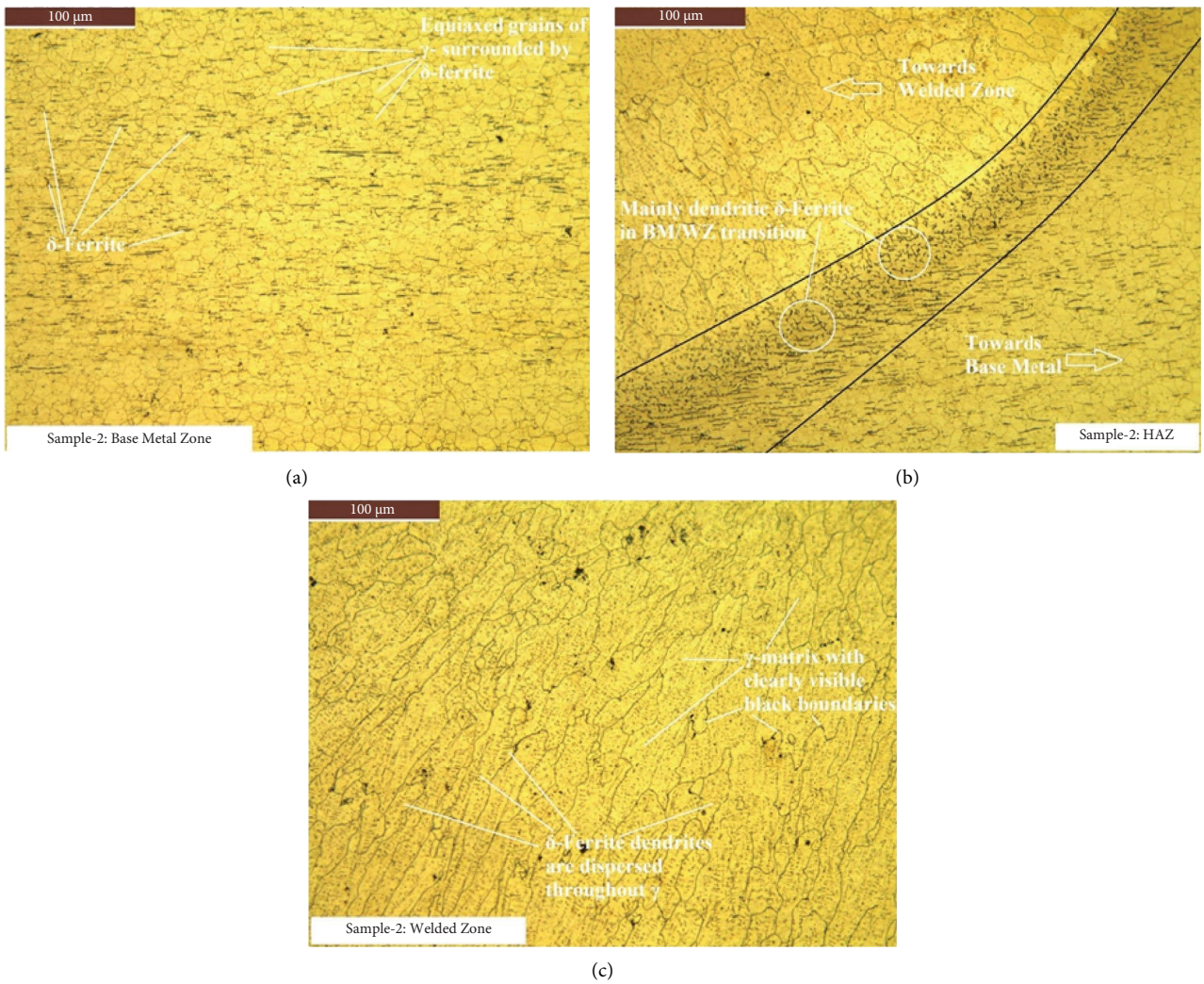

Figure 6: Microstructural appearance of sample 2 (water quenched sample): (a) the base metal, (b) HAZ, and (c) welded zone.

and coarser than that of sample 1. Twin is not visible anywhere. The appearance of δ-ferrite is somewhat like sample 1. Figure 6(b) is the HAZ of sample 2. The boundary between WZ and BM shows that the area nearer to BM is mainly containing lathy ferrite, whereas it is dendritic towards the WZ. As compared to sample 1, the ferrite dispersion in the transition zone (between WZ and BM) in sample 2 is lower and widely spaced. Figure 6(c) is the image of WZ which imparts an equiaxed γ-matrix but a little finer than that of sample 1. The γ-matrix is fully dispersed with δ-dendrites (black colored).

The grain orientation of sample 3 is shown in Figure 7. The BM is showing the coarser γ-matrix than the same of sample 2. Rest of the things is almost similar. No twin is formed in this sample also. By the virtue of slow cooling inside the sand, the WZ possesses a very coarse γ-matrix with numerous δ-ferrite as dots or tiny globules. This is the condition which improves the ductile property of austenitic steel. The HAZ (Figure 7(c)) possesses a narrow transition zone between WZ and BM. It imparts a widely spaced lamella of the γ and δ phase. Some lathy structure can also be seen in this zone.

The microstructure of sample 4 can be seen in Figure 8. The images of all the three zones are very similar to those of sample 3. Both samples 3 and 4 are tempered after quenching. Sample 4 is cooled at a relatively faster rate (medium was air). Hence, the only change was observed in the γ-matrix of the welded zone. It is comparatively finer than sample 3. The HAZ imparts lathy ferrite which is widely spread.

The grains structure of sample 5 is shown in Figure 9. This sample has more uniform γ-matrix as compared to others. The clearly defined boundaries of the γ-phase are like spherical in shape. Twin formation is completely restricted. The HAZ (Figure 9(b)) is containing both lathy and dendritic ferrite across the transition zone. The WZ is mainly containing coarse γ-matrix with dendritic appearance of δ-ferrite. All the microscopic results of this work are comparable with the same of Kellai et al. [24].

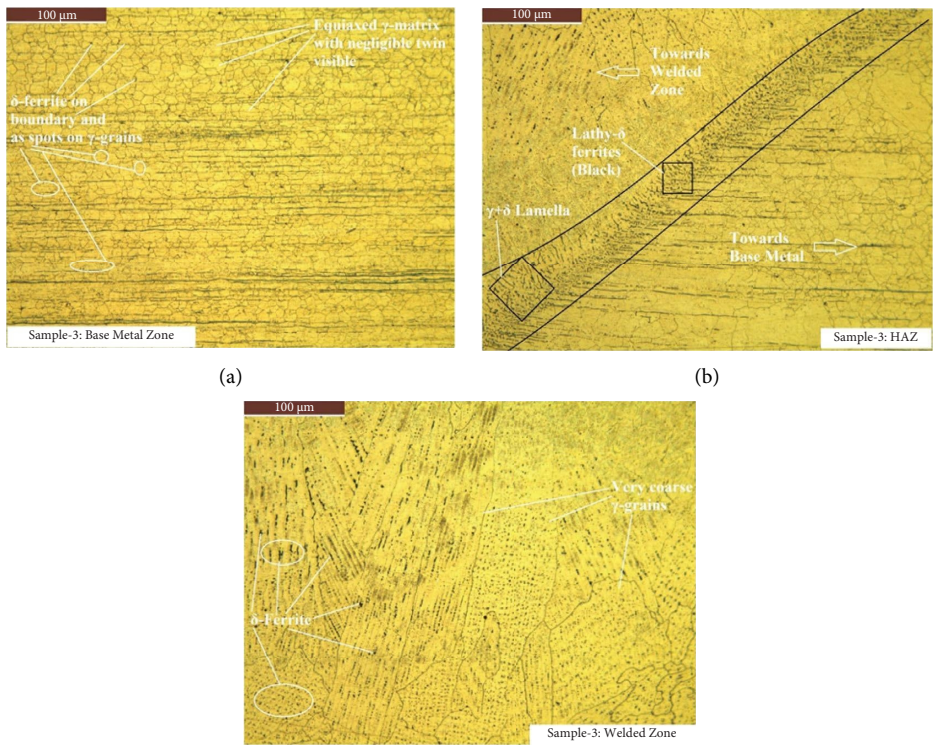

Figure 7: Microstructural appearance of sample 3 (water + sand-cooled): (a) the base metal, (b) HAZ, and (c) welded zone.

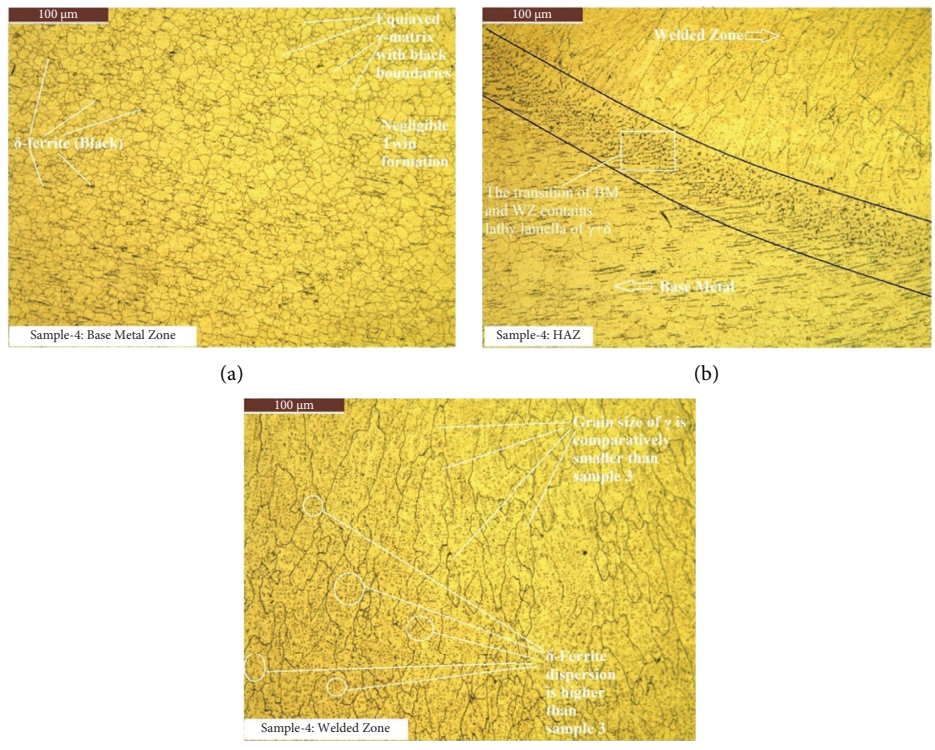

Figure 8: Microstructural appearance of sample 4 (water + air-cooled): (a) the base metal, (b) HAZ, and (c) welded zone.

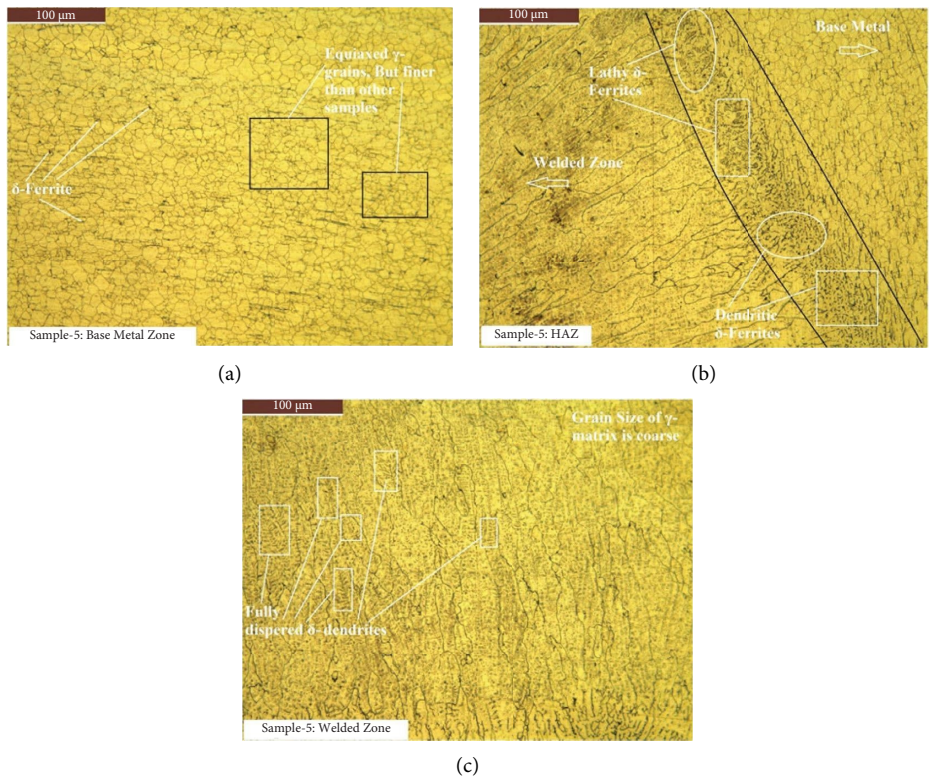

Figure 9: Microstructural appearance of sample 5, stepped cooled (sand + water-cooled): (a) the base metal, (b) HAZ, and (c) welded zone.

3.2. Tensile Test Results. The load-displacement graphs of all the samples are shown in Figure 10. The profile of all the graphs is similar. Sample 1, i.e., original sample exhibited UTS of 470 MPa at an elongation of 6.6 mm. These values are considered as the standard for comparison basis. Sample 2 had shown UTS of 434 MPa with 6.5 mm of elongation. Both the values are 7.6% and 1.5%, respectively, lower than the UTS and elongation of sample 1. Hence, only water quenching has reduced the strength and ductility of the sample. Sample 3, which was initially quenched and then tempered, had shown a UTS value of 469 MPa, which is almost same as the original sample. The elongation shown by this sample, i.e., 8.1 mm, is 23% higher than that of the original sample. Hence, the sand cooling method has improved the ductile behavior of the sample. This has happened by the coarse structure of the γ-matrix at the WZ. Unlike sample 3, sample 4 had shown a considerable reduction in elongation which is 18% less than that of the original sample. Also, it showed a UTS value of 441 MPa which is smaller that of sample 1. Sample 5 had exhibited the UTS of 437 MPa and elongation of 5.2 mm which are almost 7% and 21% lower as compared with sample 1. Hence, quick cooling through sand followed by rapid quenching has negative effects on ductility. A comparative bar chart among the UTS and elongation of five different samples is shown in Figure 10(f).

3.3. Fractography Analysis. The fracture behavior of the tensile test specimens was analyzed by FESEM images. All the images were captured at a same magnification and at same scales, i.e., 500X and 10 μm, respectively. Figure 11(a) shows the magnified fractured surface of sample 1 which was "as welded." The plastically deformed location with whirl-like appearance could be observed in the same. Some pores and dimples along with microdimples were also reported in the image. All these symptoms are of ductile failure. Sample 2 (water quenched) showed dimples and very less pores in the image. No microdimples and plastic flow could be noted (Figure 11(b)). Hence, it is comparatively less ductile than the original sample. Figure 11(c) is the fracture part of sample 3 which was mainly sand-cooled. A numerous plastically deformed zones were reported which seems like whirls. In addition, numerous microdimples, dimples, and pores were also identified. Its appearance is very similar to that of the original sample. Therefore, by the virtue of high ductility, a good elongation was achieved in sample 3 during the tensile test. Figure 11(d) is the fractography image of sample 4 which was primarily cooled in air which provided the faster cooling rate than that of sand. As a result, the plastically deformed zones were almost negligible in the image. Only dimples could be observed. These symptoms proved the less ductile behavior of sample 4. Figure 11(e) is an image of sample 5. This is the sample which was first cooled in sand then in water. Due to slow cooling at the initial stage, some plastically deformed zones were reported along with an area which was full of pores and dimples over there. Although these are the indications of good ductility, the extension provided by sample 5 during the tensile test is very less.

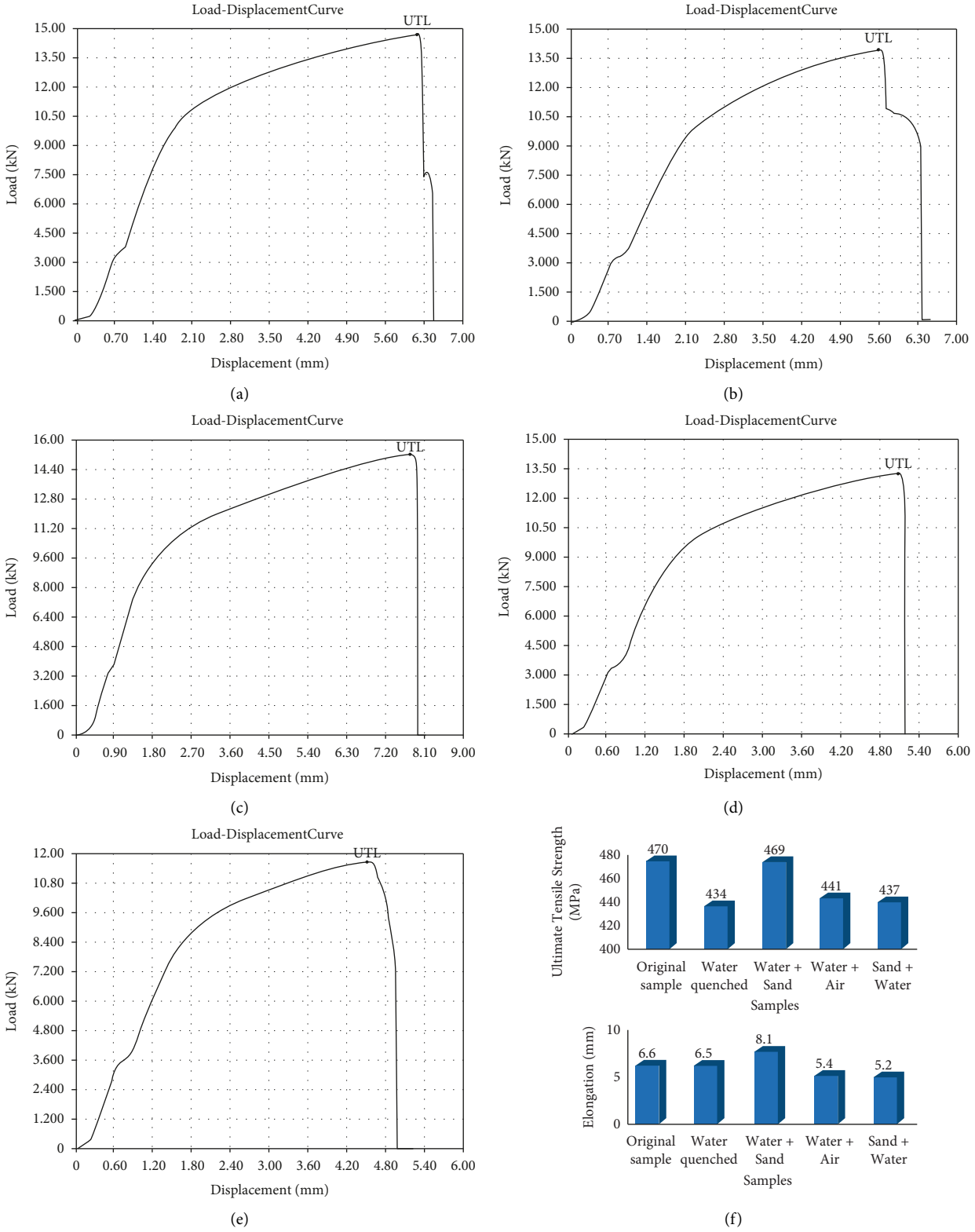

Figure 10: Load vs. displacement graphs of five specimens: (a) sample 1 (original sample); (b) sample 2 (water-quenched sample); (c) sample 3 (water + sand-cooled); (d) sample 4 (water + air-cooled); (e) sample 5 (sand + water-cooled); (f) the comparative bar chart of UTS and elongation.

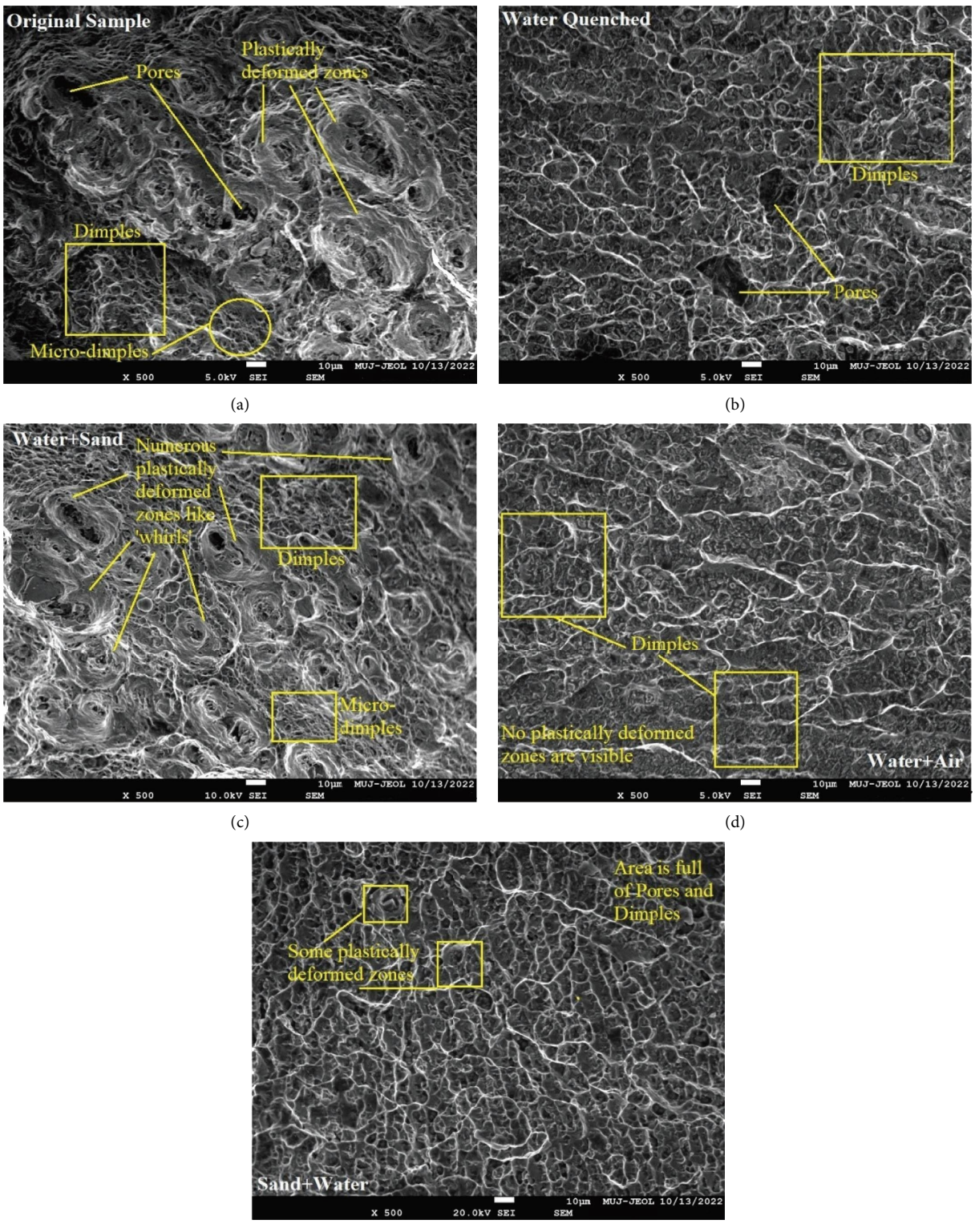

Figure 11: Fractography analysis of broken tensile test specimens.

3.4. Hardness Test Results. As already mentioned above, the Vickers microhardness test was carried out on the samples. According to the microscopic images, three zones (BM, HAZ, and WZ) were investigated for hardness variation. In each zone, three different indentations were made, and their average values were calculated. The hardness values of sample 1, sample 2, sample 3, sample 4, and sample 5 are shown in Tables 1–5, respectively.

Table 1: Microhardness values in sample 1 (original).

Sr. no.	Sample: original sample	Hardness values in HV300 gms	Average hardness (HV)
1	Base	194, 191, and 189	191.33
2	HAZ	195, 198, and 197	196.67
3	Weld	202, 197, and 209	202.67

Table 2: Microhardness values in sample 2 (water-quenched).

Sr. no.	Sample: water-quenched sample	Hardness values in HV300 gms	Average hardness (HV)
1	Base	194, 189, and 191	191.33
2	HAZ	190, 187, and 193	190
3	Weld	221, 224, and 215	220

Table 3: Microhardness values in sample 3 (tempered in water + sand).

Sr. no.	Sample: water + sand sample	Hardness values in HV300 gms	Average hardness (HV)
1	Base	223, 217, and 221	220.33
2	HAZ	224, 229, and 219	224
3	Weld	223, 217, and 226	222

Table 4: Microhardness values in sample 4 (tempered in water + air).

Sr. no.	Sample: water + air sample	Hardness values in HV300 gms	Average hardness (HV)
1	Base	207, 204, and 213	208
2	HAZ	214, 216, and 221	217
3	Weld	212, 209, and 216	212.33

Table 5: Microhardness values in sample 5 (stepped cooling sand + water).

Sr. no.	Sample: sand + water sample	Hardness values in HV300 gms	Average hardness (HV)
1	Base	199, 194, and 197	196.67
2	HAZ	204, 206, and 202	204
3	Weld	209, 199, and 205	204.33

The original sample, water-quenched sample, and stepped-cooled sample showed the highest hardness at the welded zone, whereas both the tempering processes have made the heat-affected zone harder than other parts. If only the welded zone is focused, then all the heat-treated samples had shown an increment in hardness in comparison to the original sample. The percentage improvement in hardness at the welded zone of water-quenched, water + sand-cooled, water + air-cooled, and sand + water-cooled is 9%, 10%, 5%, and 1%, respectively. A comparative bar chart of hardness, with respect to microstructure, in various zones is shown in Figure 12.

4. Discussion

The present work provides a comparative assessment among quenching, tempering (two types), and stepped heat treatment on the basis of tensile strength and hardness results along with a detailed microstructural appearance. Based on the present experimental work, a comparative analysis of mechanical properties is discussed in Table 6. The fundamental behind this work was to determine the difference between tempering and stepped heat treating. The problems generated by quenching are removed by tempering methods, but the tempering involves a repetitive work, heating, holding, and cooling again. Besides a time consuming work, this may cause high energy loss also. Hence, to find an alternative of tempering, step heat treatment has been adopted in this work. Although the results of stepped heat treatment have not been achieved satisfactorily, an idea of further improvement is developed. In future, the approach of tempering and stepped heat treatment will be significantly varied by increasing the number of samples.

Plain TIG welding may sometimes lead to formation of poor microstructures and distorted weld properties.

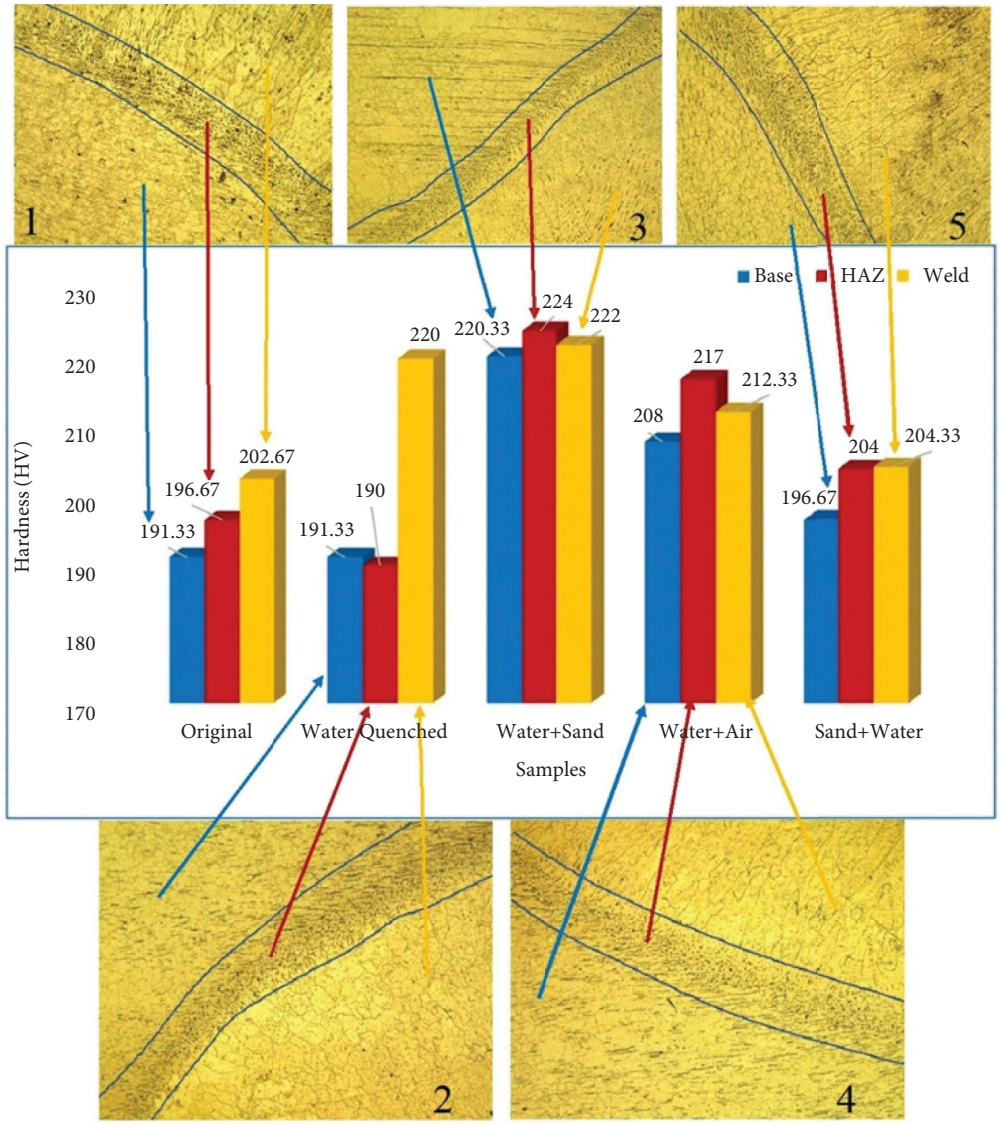

Figure 12: A comparative analysis of hardness at different parts of welded plates.

Table 6: A comparative analysis among different mechanical properties.

Samples	Ultimate tensile strength (MPa)	Elongation (mm)	Hardness		
			Base metal zone	HAZ	Welded zone
Sample 1	470	6.6	191.33	196.67	202.67
Sample 2	434	6.5	191.33	190	220
Comparative analysis with respect to sample 1	−7.6%	−1.5%	Same	−3.4%	9%
Sample 3	469	8.1	220.33	224	222
Comparative analysis with respect to sample 1	−0.2%	23%	15%	14%	10%
Sample 4	441	5.4	208	217	212.33
Comparative analysis with respect to sample 1	−6.1%	−18%	9%	10%	5%
Sample 5	437	5.2	196.67	204	204.33
Comparative analysis with respect to sample 1	−7%	−21%	3%	4%	1%

The idea of using a filler metal in keyhole-TIG has overcome the problem of poor properties. As suggested by Fei et al. [25] and Su et al. [26], the use of the filler material has remarkably enhanced the capability of the keyhole-TIG process.

5. Conclusion

An attempt has been made to critically analyze the microstructure, tensile strength, and hardness of the TIG-welded joints in SS-304 plates with and without heat-treated

conditions. Also, a comparative measure has been provided to find out the suitable heat treatment process. The following conclusion can be drawn:

(i) The tensile strength of SS-304-welded joint gets reduced after heat treatment. A reduction of 7.6%, 0.2%, 6.1%, and 7% in tensile strength was observed in sample 2, sample 3, sample 4, and sample 5, respectively, although the sample 3 (quick water sprinkle + sand cooling process) has a comparable result with that of the original sample.

(ii) The tempering process has significantly improved the ductility of the sample. It has been established by virtue of 23% enhancement in elongation of sample 3. However, other treatments have shown a negative result on elongation.

(iii) As per the hardness test results, all the heat treatments have increased the hardness of the welded joint which is nearly 9%, 10%, 5%, and 1% improvement in sample 2, sample 3, sample 4, and sample 5, respectively.

(iv) The heat treatment has made significant changes in the microstructural appearance of the samples. As soon as the cooling becomes faster, the δ-ferrite gets precipitated in the form of dendrites. The third sample, which was primarily cooled in sand, has shown very coarse γ-grains with δ-ferrites dispersed as dots throughout it. The heat treatment has created a widely spaced lathy structure and a less dendritic structure of δ-ferrite in the HAZ. In base metal parts, the heat treatment has made the γ-matrix coarse and equiaxed. Also, twin formation is restricted due to heat treatment.

Data Availability

All the data used to support the findings of this study are included within the article.

Conflicts of Interest

The authors declare that they have no conflicts of interest.

References

[1] W. D. Callister and D. G. Rethwisch, *Materials Science and Engineering: An Introduction*, John Wiley and Sons, New York, NY, USA, 10th edition, 2018.

[2] S. Dewangan and S. Chattopadhyaya, "Analysing effect of quenching and tempering into mechanical properties and microstructure of 304-SS welded plates," *Acta Metallurgica Slovaca*, vol. 28, no. 3, pp. 140–146, 2022.

[3] T. S. Balasubramanian, M. Balakrishnan, V. Balasubramanian, and M. M. Manickam, "Influence of welding processes on microstructure, tensile and impact properties of Ti-6Al-4V alloy joints," *Transactions of Nonferrous Metals Society of China*, vol. 21, no. 6, pp. 1253–1262, 2011.

[4] D. K. Gope, U. Kumar, S. Chattopadhyaya, and S. Mandal, "Experimental investigation of pug cutter embedded TIG welding of Ti-6Al-4V titanium alloy," *Journal of Mechanical Science and Technology*, vol. 32, no. 6, pp. 2715–2721, 2018.

[5] G. Lütjering, J. C. Williams, and A. Gysler, "Microstructure and mechanical properties of titanium alloys," *Microstructure And Properties Of Materials*, vol. 2, pp. 1–77, 2000.

[6] J. Józwik, D. Ostrowski, R. Milczarczyk, and G. Krolczyk, "Analysis of relation between the 3D printer laser beam power and the surface morphology properties in Ti-6Al-4V titanium alloy parts," *Journal of the Brazilian Society of Mechanical Sciences and Engineering*, vol. 40, no. 4, p. 215, 2018.

[7] U. Kumar, D. K. Gope, R. Kumar et al., "Investigation of microstructure and mechanical properties of titanium alloy sheet using low power Nd-YAG laser welding process," *Metallic Materials*, vol. 56, no. 02, pp. 121–129, 2018.

[8] Z. Zhang, H. Zhang, J. Hu et al., "Microstructure evolution and mechanical properties of briefly heat treated SAF 2507 super duplex stainless steel welds," *Construction and Building Materials*, vol. 168, pp. 338–345, 2018.

[9] A. Järvenpää, M. Jaskari, M. Keskitalo, K. Mäntyjärvi, and P. Karjalainen, "Microstructure and mechanical properties of laser-welded high- strength AISI 301LN steel in reversion-treated and temper-rolled conditions," *Procedia Manufacturing*, vol. 36, pp. 216–223, 2019.

[10] B. Sadeghi, H. Sharifi, M. Rafiei, and M. Tayebi, "Effects of post weld heat treatment on residual stress and mechanical properties of GTAW: the case of joining A537CL1 pressure vessel steel and A321 austenitic stainless steel," *Engineering Failure Analysis*, vol. 94, pp. 396–406, 2018.

[11] S. Dewangan, N. Mainwal, M. Khandelwal, and P. S. Jadhav, "Performance analysis of heat treated AISI 1020 steel samples on the basis of various destructive mechanical testing and microstructural behaviour," *Australian Journal of Mechanical Engineering*, vol. 20, no. 1, pp. 74–87, 2022.

[12] U. Kumar, D. Gope, J. Srivastava, S. Chattopadhyaya, A. Das, and G. Krolczyk, "Experimental and numerical assessment of temperature field and analysis of microstructure and mechanical properties of low power laser annealed welded joints," *Materials*, vol. 11, no. 9, p. 1514, 2018.

[13] A. Królicka, K. Radwański, A. Janik, P. Kustroń, and A. Ambroziak, "Metallurgical characterization of welded joint of nanostructured bainite: regeneration technique versus post welding heat treatment," *Materials*, vol. 13, no. 21, p. 4841, 2020.

[14] M. N. Brykov, I. Petryshynets, M. Džupon et al., "Microstructure and properties of heat affected zone in high-carbon steel after welding with fast cooling in water," *Materials*, vol. 13, no. 22, p. 5059, 2020.

[15] M. Ahonen, R. Mouginot, T. Sarikka et al., "Effect of thermal ageing at 400 °C on the microstructure of ferrite-austenite interface of nickel-base alloy narrow-gap dissimilar metal weld," *Metals*, vol. 10, no. 3, p. 421, 2020.

[16] T. Wang, S. S. Ao, S. M. Manladan, Y. C. Cai, and Z. Luo, "Microstructure and properties of surface-modified plates and their welded joints," *Materials*, vol. 12, no. 18, p. 2883, 2019.

[17] S. Baskutis, J. Baskutiene, R. Bendikiene, A. Ciuplys, and K. Dutkus, "Comparative research of microstructure and mechanical properties of stainless and structural steel dissimilar welds," *Materials*, vol. 14, no. 20, p. 6180, 2021.

[18] H. Zhang, Q. Chang, J. Liu, H. Lu, H. Wu, and J. Feng, "A novel rotating wire GMAW process to change fusion zone shape and microstructure of mild steel," *Materials Letters*, vol. 123, pp. 101–103, 2014.

[19] S. Geng, J. Sun, L. Guo, and H. Wang, "Evolution of microstructure and corrosion behavior in 2205 duplex stainless

steel GTA-welding joint," *Journal of Manufacturing Processes*, vol. 19, pp. 32–37, 2015.

[20] T. A. Tabish, T. Abbas, M. Farhan, S. Atiq, and T. Z. Butt, "Effect of Heat Input on Microstructure and Mechanical Properties of the TIG Welded Joints of AISI 304 Stainless Steel," *International Journal of Scientific & Engineering Research*, vol. 5, no. 7, 2014.

[21] P. Wang, Y. Zhang, and D. Yu, "Microstructure and mechanical properties of pressure-quenched SS304 stainless steel," *Materials*, vol. 12, no. 2, p. 290, 2019.

[22] J. Yan, M. Gao, and X. Zeng, "Study on microstructure and mechanical properties of 304 stainless steel joints by TIG, laser and laser-TIG hybrid welding," *Optics and Lasers in Engineering*, vol. 48, no. 4, pp. 512–517, 2010.

[23] M. Dadfar, M. H. Fathi, F. Karimzadeh, M. R. Dadfar, and A. Saatchi, "Effect of TIG welding on corrosion behavior of 316L stainless steel," *Materials Letters*, vol. 61, no. 11-12, pp. 2343–2346, 2007.

[24] A. Kellai, S. Kahla, S. Dehimi, L. Kaba, and Z. Boutaghou, "Effect of post weld heat treatment on the microstructure and mechanical properties of a gas-tungsten-arc-welded 304 stainless steel," *The International Journal of Advanced Manufacturing Technology*, vol. 121, no. 11-12, pp. 8171–8186, 2022.

[25] Z. Fei, Z. Pan, D. Cuiuri, H. Li, B. Wu, and L. Su, "Improving the weld microstructure and material properties of K-TIG welded armour steel joint using filler material," *International Journal of Advanced Manufacturing Technology*, vol. 100, no. 5-8, pp. 1931–1944, 2019.

[26] L. Su, Z. Fei, B. Davis, H. Li, and H. Bornstein, "Digital image correlation study on tensile properties of high strength quenched and tempered steel weld joints prepared by K-TIG and GMAW," *Materials Science and Engineering: A*, vol. 827, Article ID 142033, 2021.